Low-Complexity Layered ACO-OFDM for Power-Efficient Visible Light Communications

Ruowen Bai, *Graduate Student Member, IEEE*, Steve Hranilovic, *Fellow, IEEE*, and Zhaocheng Wang, *Fellow, IEEE*

***Abstract*—Commercially available LED luminaires demand both low-complexity and high power efficiency from visible light communication (VLC) deployments. Layered asymmetrically clipped optical orthogonal frequency division multiplexing (LACO-OFDM) is attracting increasing interest due to the high spectral efficiency and high power efficiency. However, these advantages come at the price of high computational complexity at both transmitter and receiver. In this paper, we propose a low-complexity LACO-OFDM (L-LACO) to generating identical signals to conventional systems while employing a half-size IFFT/FFT and possessing low implementation complexity. The required number of real-valued multiplication operations and real-valued addition operations are quantified and compared to conventional LACO-OFDM. The saved power corresponding to the reduction in arithmetic operations is also estimated, which is shown to increase logarithmically with number of subcarriers, and to increase linearly with modulation bandwidth. Numerical results show that the proposed L-LACO requires about half the number of arithmetic operations as LACO-OFDM for both the transmitter and the receiver. The BER performance of L-LACO is estimated by Monte Carlo simulations under a VLC line-of-sight (LOS) channel and under a VLC dispersive channel that is shown to be identical to LACO-OFDM.**

***Index Terms*—Visible light communication, low complexity, OFDM, ACO-OFDM, LACO-OFDM.**

I. Introduction

A. Introduction, Related Work and Motivation

VISIBLE light communication (VLC) for indoor communications has been touted as a promising complementary link to conventional wireless radio frequency (RF) communication due to the ubiquity of solid-state illumination and large amounts of unregulated visible light spectrum [1]–[3]. An underlying constraint in any VLC system based on commercial luminaires is that the complexity and power consumption of any processing must be minimized to preserve energy efficiency. As a result, intensity modulation with direct detection (IM/DD) is typically employed in VLC links thanks to its low complexity [4]–[6]. The data are modulated onto the instantaneous optical intensity emitted by a light-emitting diode (LED), where the average optical power corresponds to the average LED driving current. Hence, the input signal must be real-valued and non-negative [1]–[7]. At the receiver, a photodiode (PD) is used to convert the received optical signal to an electrical current, which is assumed to be proportional to the received optical power.

In VLC channels, orthogonal frequency division multiplexing (OFDM) has been investigated intensely to enhance data rate and power efficiency due to its inherent benefits including high spectral efficiency, resistance to frequency-selective channels, and simple one-tap equalization [8]–[11]. In order to produce a real-valued signal compatible with IM/DD, Hermitian symmetry is generally induced in the frequency domain [11]–[14]. Further, to achieve non-negative output amplitudes, direct current (DC) biased optical OFDM (DCO-OFDM) requires a large DC bias and all the remaining negative peaks are clipped at zero [15]. The required DC bias consumes much optical power but carries no information.

To improve optical power efficiency, asymmetrically clipped optical OFDM (ACO-OFDM) [15], [16], pulse-amplitude-modulated discrete multitone (PAM-DMT) [17], unipolar OFDM (U-OFDM) [18] and Flip-OFDM [19], antisymmetry-constructed clipped optical OFDM (AC-OFDM) [20] were proposed; however, these optical power efficient OFDM schemes have a drawback of achieving only half the spectral efficiency as DCO-OFDM. To enhance the spectral efficiency and to retain optical power efficiency, layered spectrum efficient OFDM schemes such as enhanced U-OFDM (eU-OFDM) [18], enhanced ACO-OFDM (eACO-OFDM) [21], spectral and energy efficient OFDM (SEE-OFDM) [22], layered ACO-OFDM (LACO-OFDM) [23], and enhanced ACO-OFDM (EACO-OFDM) [24] were then proposed independently. These spectrum efficient OFDM schemes superimpose several layers/streams, which are transmitted at the same time. These multiple-layer/stream OFDM schemes are in a similar philosophy to LACO-OFDM while proposed independently.

Recently, there has been intense research on LACO-OFDM, including improved detection performance [4], [25]–[29], reduction in peak-to-average power ratio (PAPR) [9], [30]–[32], capacity analysis [14], [33]–[35], investigation of channel coding performance [36]–[39], dimming [40]–[43], enhanced spectral efficiency [14], [44]–[48], experimental demonstrations [47], [49]–[51], decreased computational complexity [20], [22], [49], [52], [53], and explicit

Manuscript received 27 September 2021; revised 6 December 2021 and 18 January 2022; accepted 25 January 2022. Date of publication 31 January 2022; date of current version 19 August 2022. This work was supported by the Natural Sciences and Engineering Research Council of Canada. The associate editor coordinating the review of this article and approving it for publication was H. Tabassum. *(Corresponding author: Steve Hranilovic.)*

Ruowen Bai and Steve Hranilovic are with the Department of Electrical and Computer Engineering, McMaster University, Hamilton, ON L8S 4L8, Canada (e-mail: bair4@mcmaster.ca; hranilovic@mcmaster.ca).

Zhaocheng Wang is with the Department of Electronic Engineering, Tsinghua University, Beijing 100084, China (e-mail: zcwang@tsinghua.edu.cn).

Digital Object Identifier 10.1109/TGCN.2022.3147970

TABLE I
RECENT RESEARCH ON LACO-OFDM

Topics and Directions	Relevant Recent Researches
Detection performance	[4] An improved receiver with residual clipping noise mitigation [25] An improved receiver using pairwise detection for noise cancellation [26] A new receiver using diversity combining over both flat and frequency-selective channels [27] A diversity combining receiver achieving up to 2 dB electrical gains [28] A two-stage receiver using soft interference cancellation and noise clipping realizing up to 2.43 dB gains [29] A multi-stage improved receiver to mitigate the clipping noise due to dynamic range of electrical and optical components
PAPR reduction	[9] Performance analysis & PAPR reduction [30] Proposes layered/enhanced asymmetrically clipped optical single-carrier frequency-division multiplexing (L/E-ACO-SCFDM) based on discrete Hartley transform with PAPR reduction up to 4.2 dB [31] Proposes interleaved discrete-Fourier-transform-spread layered/enhanced ACO-OFDM (IDFTS-L/e-ACO) with PAPR reduction up to 7.5 dB [32] Proposes a cyclic shifted LACO-OFDM (CS-LACO-OFDM) with PAPR reduction up to 2.5 dB
Capacity analysis	[14] Analyses, optimises (using convex optimization techniques) and compares the achievable information rate of optical OFDM modulation schemes in an IM/DD channel with Gaussian noise [33] Proposes adaptive LACO-OFDM and analyses capacity with optimal layer [34] Analyses comparatively the capacity of unipolar OFDM schemes in Gaussian optical intensity channel [35] Analyses and optimises discrete-input continuous-output memoryless channel (DCMC) capacity of LACO-OFDM [55] Analyses and compares achievable rate of multi-carrier modulation schemes for bandlimited IM/DD Systems
Channel coding	[36] Pairwise coding to mitigate error propagation between layers [37] Analyses capacity and integrates forward error correction (FEC) codes to LACO-OFDM for BER improvement [38] Designs a multilayered code that trades spectral efficiency for BER improvement [39] Multilayered channel coding with experiment verification
Dimming control	[40] Dimmable LACO-OFDM with wide dimming range [41] Spatial-domain and time-domain dimming control for LACO-OFDM [42] Dimmable L/E-ACO-SCFDM [43] Dimmable reconstructed LACO-OFDM (RLACO-OFDM)
Spectral efficiency	[14], [44] Proposes ALACO-OFDM that can be more spectral efficient than LACO-OFDM with fewer layers [45] Proposes triple-layer hybrid optical OFDM (THO-OFDM) that can be more spectral efficient than LACO-OFDM with three layers [46] Proposes hybrid non-orthogonal multiple access (NOMA) and orthogonal multiple access (OMA) for LACO-OFDM performance improvement [47] Proposes hierarchical pre-distorted LACO-OFDM (HPD-LACO-OFDM) for NOMA performance improvement [48] Proposes flexible NOMA-based non-orthogonal hybrid optical OFDM (NOHO-OFDM) scheme
Experimental demo.	[49] Demonstrates an experiment based field-programmable gate arrays (FPGA) with low-complexity transmitter [47] Demonstrates a point-to-point transmission experiment [50] Demonstrates worst-case residual clipping noise power model for bit-loading in LACO-OFDM [51] Demonstrates a short-haul optical fiber link using layered/enhanced ACO-OFDM
Complexity reduction	[22], [52] Proposes a low-complexity receiver for using a single FFT module sacrificing about $2-3$ dB power [49] focuses on a high-efficient implementation from the hardware prospect and improves L/E-ACO-OFDM transmitter [20], [53] Proposes LAC-OFDM saving half arithmetic operations while achieving same BER performance as LACO-OFDM under a VLC LOS flat channel
Bandlimited signals	[54] Simulates LACO-OFDM BER performance for a strictly bandlimited VLC system [55] Analyses achievable rate of multi-carrier modulation schemes, including SEE-OFDM, and proposes filtered SEE-OFDM (FSEE-OFDM) for bandlimited IM/DD systems

consideration of bandwidth constraints [54], [55]. For readability, these research papers are summarized and contrasted in Table I.

Though spectrally efficient, the use of multiple layers/streams of OFDM modulation schemes suffers from increased computational complexity [56], which is especially significant for cost and power-constrained VLC luminaires. Hardware-efficient layered/enhanced ACO-OFDM (L/E-ACO-OFDM) was proposed in [49], and focuses on a highly efficient implementation from a hardware perspective and creatively improves L/E-ACO-OFDM transmitter by modifying the inverse fast Fourier transform (IFFT) implementation that calculates only the bottom half in the IFFT butterfly. However, the approach only applies to the transmitter, and the receiver remains highly complex. A low-complexity receiver using a single fast Fourier transform (FFT) module for LACO-OFDM is investigated in [52], which reduces the complexity of the receiver at the expense of about $2-3$ dB power loss at a bit error rate (BER) of 10^{-3}. More recently, layered AC-OFDM (LAC-OFDM) is proposed for VLC line-of-sight (LOS) channels, which is low-complexity thanks to employing half-size IFFT and half-size FFT while retaining the same optical power efficiency as LACO-OFDM [20]. However, an additional N-point FFT and N-point IFFT are additionally required to implement frequency domain equalization (FDE) when LAC-OFDM is employed on a dispersive VLC channel. To summarize, only a few papers have considered the reduction of computation complexity at both the transmitter and the receiver while retaining the spectral- and power efficiency simultaneously, which is a key motivation of this work.

B. Novelty and Contributions

In this paper, we propose low-complexity ACO-OFDM (L-ACO-OFDM, termed as L-ACO hereafter), which generates identical signals to conventional ACO-OFDM while employing an IFFT that is only half the size of ACO-OFDM. To enhance the spectral efficiency, low-complexity LACO-OFDM (L-LACO-OFDM, termed as L-LACO hereafter) is

TABLE II
CONTRAST BETWEEN METHODOLOGY ADOPTED IN [49] AND L-LACO

	Ref. [49]	**L-LACO**
Complexity reduction at transmitter	Half	Half
Complexity reduction at receiver	Same complexity as LACO-OFDM receiver	Half
The IFFT size in the l-th layer	Same size as IFFT at LACO-OFDM transmitter	Half size as IFFT at LACO-OFDM transmitter
$\mathcal{R}$-radix IFFT butterfly	$\mathcal{R} = 2$	$\mathcal{R}$ could be any divisor of N
The need for modifying IFFT algorithm	Modifies the IFFT implementation that calculates only the bottom half in the IFFT butterfly.	No need. A common IFFT is good.

proposed, which combines L layers of L-ACO signals to generate identical OFDM signals as LACO-OFDM in [23]. The size of the IFFT/FFTs employed in each layer are half the size needed in LACO-OFDM. Hence L-LACO is far less-complex as compared to LACO-OFDM at both the transmitter and receiver. The power savings due to the reduced computation compared to LACO-OFDM are estimated at both transmitter and receiver. Additionally, the BER performance of the proposed L-LACO is estimated by Monte Carlo simulations under a VLC line-of-sight (LOS) channel and a VLC dispersive channel, respectively. The simulation results show that L-LACO achieves the identical performance compared to LACO-OFDM. Therefore, L-LACO generates spectrally efficient LACO-OFDM using half-size IFFT/FFT at transmitter and receiver, which is essential for complexity and energy constrained VLC systems.

Compared to the methodology adopted in [49] that modifies the IFFT implementation by calculating only the bottom half in the IFFT butterfly, L-LACO does not need to modify any IFFT butterfly structure. In [49], a 2-radix IFFT butterfly is required to save half the complexity compared to the LACO-OFDM transmitter. In contrast, a common IFFT with $\mathcal{R}$-radix butterfly could be utilized to save half-complexity where $\mathcal{R}$ could be any divisor of the number of subcarriers N. In [49], the size of IFFT in each layer remains the same as conventional LACO-OFDM. In contrast, L-LACO employs half-size IFFT as conventional LACO-OFDM in each layer. Additionally, [49] only decreases the complexity of the L/e-ACO-OFDM transmitter. The receiver still requires as high computational complexity as conventional LACO-OFDM. In contrast, our proposed L-LACO decreases the complexity of the LACO-OFDM transmitter and the receiver by nearly half. The contrast between the methodology adopted in [49] and that adopted in L-LACO is summarized in Table II.

The main contributions of this paper can be summarised as:

- Firstly, this paper proposes L-LACO to design the entire transceiver. L-LACO is shown mathematically to generate identical signals as conventional LACO-OFDM while its transceiver is less complex. The L-LACO transmitter utilizes a half-size IFFT in each layer as conventional LACO-OFDM transmitter, and L-LACO receiver utilizes half-size IFFT and half-size FFT in each iteration as conventional LACO-OFDM receiver.
- Secondly, we analyse the computational complexity of both transmitter and receiver quantitatively. This work quantifies the required number of real-valued multiplication operations (RMOs) and real-valued addition operations (RAOs) for L-LACO transceiver and conventional LACO-OFDM. Numerical results support the theoretical analysis of the computational complexity reduction.
- Thirdly, this work quantifies the saved power of the L-LACO transmitter and receiver as compared to conventional LACO-OFDM. Numerical results are aligned well with our theoretical analysis on saved power.
- Finally, this work presents the BER performance of L-LACO and conventional LACO-OFDM under both VLC LOS and dispersive channels. Numerical results show that L-LACO has the identical BER as LACO-OFDM, however, requires about half the number of arithmetic operations.

C. Paper Structure

The remainder of this paper is organized as follows. Section II briefly introduces VLC channel model and conventional ACO-OFDM and LACO-OFDM, while the proposed L-ACO and L-LACO are presented in Sections III and IV, respectively. Computational complexity is analysed in Section V. Numerical results are presented in Section VI. Finally, conclusions are drawn in Section VII.

Notations: In this paper, N denotes the number of subcarriers. Additionally, we use an uppercase letter, e.g., Y and its bold form, e.g., $\boldsymbol{Y}$ to denote a frequency-domain scalar and vector signal while a lowercase letter, e.g., y and its bold form, e.g., $\boldsymbol{y}$ denote a time-domain scalar and vector signal, respectively. Note Y^* denotes complex conjugate of a complex number Y. Furthermore, $\mathrm{mod}(\cdot,\cdot)$ denotes modulo operation. $|\cdot|$ denotes magnitude of a complex number or absolute value of a real number. Specifically, notation symbols with the corresponding definitions and meaning utilized throughout the paper are listed in Table III.

II. BACKGROUND

A. VLC Channel Model

For a VLC LOS link, the channel is assumed to be flat with a gain H_{LOS} as [7]

$$H_{\mathrm{LOS}} = \begin{cases} \frac{\eta A_{\mathrm{PD}}(m+1)}{2\pi d^2}\cos^m(\psi)\cos(\theta), & 0 \le \theta \le \Theta_{\mathrm{F}}, \\ 0, & \text{Otherwise}, \end{cases} \quad (1)$$

where η is optical-to-electrical (O/E) conversion coefficient, A_{PD} is the effective collection area of the PD, ψ is the angle of irradiance with respect to LED axis, θ is the angle of incidence with respect to PD axis, Θ_{F} is field of view (FOV), d is the distance between LED and PD surfaces, and $m = -\ln(2)/\ln(\cos(\Psi_{1/2}))$ is the order of Lambertian emission and $\Psi_{1/2}$ is LED semi-angle. Without loss of generality, the receiver filter is assumed to be rectangular with optical power gain setting to unit.

TABLE III
KEY NOTATIONS AND SYMBOL DEFINITIONS

Notation	Eq.	Definition and Meaning
W_N	(3)	The first entry in IDFT matrix
$\boldsymbol{Y}$	(4)	Input symbol vector to N-point IFFT for ACO-OFDM
$\mathbf{y}$	(5)	Output symbol vector of N-point IFFT for ACO-OFDM
$\boldsymbol{X}$	(9)	Input symbol vector to $N/2$-point IFFT for L-ACO
$\boldsymbol{x}$	(9)	Output symbol vector of $N/2$-point IFFT for L-ACO
$\mathbf{y}_{\mathrm{c}}$	(10)	ACO-OFDM signal after clipping
$\boldsymbol{c}$	(10)	ACO-OFDM clipping distortion (CD)
$N_{\mathrm{AC}}(1)$	(11)	IFFT size of the first layer L-ACO
$\mathbf{Y}_L^{(l)}$	(12)	Input symbol vector to N-point IFFT for the l-th layer
$\mathbf{X}^{(l)}$	(15)	Input symbol vector to $N_{\mathrm{AC}}(l)$-point IFFT for the l-th layer
$\mathbf{x}^{(l)}$	(15)	Output symbol vector of $N_{\mathrm{AC}}(l)$-point IFFT for the l-th layer
$\mathbf{y}^{(l)}$	(13)	Anti-symmetric signal vector with length of $2N_{\mathrm{AC}}(l)$ in the l-th layer
$\boldsymbol{s}^{(l)}$	(13)	$s_n^{(l)} = \frac{1}{\sqrt{2^l}} W^n_{\frac{N}{2^{l-1}}}$, constant in the l-th layer
$\boldsymbol{v}^{(l)}$	(13)	$v_n^{(l)} = s_n^{(l)} x_n^{(l)}$, real-valued signal in the l-th layer
$\mathbf{y}_{\mathrm{c}}^{(l)}$	(16)	Symbol vector generated by clipping $\mathbf{y}^{(l)}$ at zero
$\boldsymbol{c}^{(l)}$	(16)	$c_n^{(l)}$, time-domain CD induced by the l-th layer
$\boldsymbol{C}^{(l)}$	(26)	$C_k^{(l)}$, CD falling onto k-th subcarrier induced by the l-th layer
$\mathbf{x}_{\mathrm{a}}^{(l)}$	(27)	$x_{\mathrm{a},n}^{(l)}$, absolute value of $x_n^{(l)}$
$\mathbf{X}_{\mathrm{a}}^{(l)}$	(27)	DFT of $\mathbf{x}_{\mathrm{a}}^{(l)}$
$\widetilde{\boldsymbol{X}}^{(l)}$	(28)	Estimate of $\boldsymbol{X}^{(l)}$ after removing CD
$\widehat{\boldsymbol{X}}^{(l)}$	(29)	Detected symbols from $\widetilde{\boldsymbol{X}}^{(l)}$
$\widehat{\boldsymbol{C}}^{(l)}$	(28)	Reconstructed CD in frequency domain based on detected symbols $\widehat{\boldsymbol{X}}^{(l)}$
$\widehat{\boldsymbol{x}}_{\mathrm{a}}^{(l)}$	(27)	Reconstructed CD based on detected symbols $\widehat{\boldsymbol{X}}^{(l)}$
$\widehat{\boldsymbol{X}}_{\mathrm{a}}^{(l)}$	(27)	DFT of $\widehat{\boldsymbol{x}}_{\mathrm{a}}^{(l)}$

Indoor VLC dispersive channels include both LOS link and diffuse components that can be well estimated by a close-form function as [7], [57]

$$h(t) = H_{\mathrm{LOS}} \frac{\tau_0^6}{(t+\tau_0)^7} u(t) \tag{2}$$

where $u(t)$ is the unit step function, $\tau_0 = 2H/c$, H is height of room, and c is speed of light [7], [57].

B. Conventional ACO-OFDM and LACO-OFDM

In ACO-OFDM, the output time-domain signal vector has an inherent anti-symmetry due to loading data on only odd subcarriers [15]. To achieve non-negativity, the negative parts are clipped at zero without any loss of information [15]. This clipping distortion (CD) falls onto even subcarriers, which are orthogonal to data-carrying subcarriers. Hence, symbols can be detected successfully on the odd subcarriers at the receiver [15].

To enhance the spectral efficiency, LACO-OFDM uses L layers of ACO-OFDM signals which are superimposed and transmitted simultaneously [23]. These L layers modulate symbols onto disjoint sets of subcarriers and each layer has an anti-symmetry. At the receiver, LACO-OFDM is demodulated successively layer by layer [23].

III. Low-Complexity ACO-OFDM

For completeness, define [58]

$$W_N = \exp\left\{\frac{j2\pi}{N}\right\} \tag{3}$$

where N is size of IFFT and FFT and $j = \sqrt{-1}$.

Conventional ACO-OFDM with N subcarriers requires an N-point IFFT at transmitter. Hermitian symmetry is required to generate real-valued signals and only odd subcarriers are utilized to carry data leading to anti-symmetric output of an IFFT. Hence the input frequency-domain symbol vector to the IFFT for ACO-OFDM is

$$\mathbf{Y} = [0, Y_1, 0, Y_3, 0, \ldots, 0, Y_3^*, 0, Y_1^*] \tag{4}$$

where Y_k denotes M-ary quadrature amplitude modulation (QAM) symbols and $(\cdot)^*$ denotes complex conjugate. The resulting time-domain output of IFFT is thus

$$y_n = \frac{1}{\sqrt{N}} \sum_{k=0}^{N-1} Y_k W_N^{nk}, \ 0 \le n \le N-1. \tag{5}$$

Notice that $\mathbf{y}$ has an inherent anti-symmetry due to the modulation of only odd subcarriers, i.e., [15]

$$y_n = -y_{n+N/2}, \ 0 \le n \le N/2 - 1. \tag{6}$$

Conventional ACO-OFDM requires high computational complexity due to the usage of N-point IFFT according to (5). In the following, we show that a half-size IFFT can be employed to generate the identical signal $\mathbf{y}$ in (6). Following the philosophy of AC-OFDM [20], where anti-symmetry is introduced in the time domain, $\mathbf{y}$ can be written as

$$\mathbf{y} = [\mathbf{v}, -\mathbf{v}] \tag{7}$$

where $\mathbf{v}$ is an $\frac{N}{2}$-length vector with the n-th element given by

$$v_n = s_n x_n \tag{8}$$

where $s_n = \frac{1}{\sqrt{2}} W_N^n$ and

$$x_n = \frac{1}{\sqrt{N/2}} \sum_{q=0}^{\frac{N}{2}-1} X_q W_{\frac{N}{2}}^{nq}, \ 0 \le n \le N/2 - 1 \tag{9}$$

where $X_q = Y_{2q+1}$ and $q = 0, \ 1, \ldots, N/2 - 1$. Notice that (9) is an $\frac{N}{2}$-point IFFT. Therefore, a conventional ACO-OFDM signal $\mathbf{y}$ in (7) can be constructed by computing $\mathbf{v}$ using an $\frac{N}{2}$-point IFFT and imposing anti-symmetry in time-domain (which requires no additional arithmetic operations). It is worth noting that v_n is a real-valued signal though x_n is not necessarily real-valued.

To satisfy the non-negativity requirement, the negative part of $\mathbf{y}$ is clipped at zero leading to $\mathbf{y}_{\mathrm{c}}$ with the n-th element given as [15]

$$y_{\mathrm{c},n} = \frac{1}{2} y_n + c_n, 0 \le n \le N-1 \tag{10}$$

where $c_n = \frac{1}{2}|y_n|$ is CD falling onto even subcarriers only, which is orthogonal to the data-bearing (i.e., odd) subcarriers in the frequency domain.

It is worth to noting that L-ACO signal $y_{\mathrm{c},n}$ generated by an N/2-point IFFT is identical to conventional ACO-OFDM signal generated by an N-point IFFT. Therefore, at the receiver side, symbols can be detected on the odd subcarriers using conventional ACO-OFDM demodulator proposed in [16].

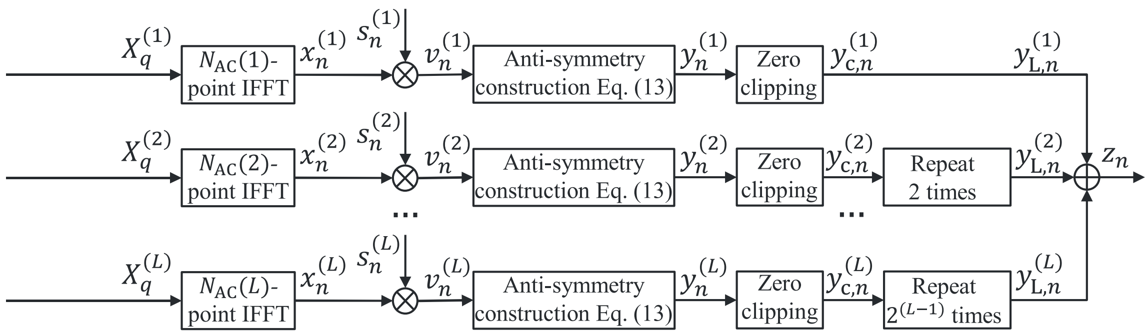

Fig. 1. Transmitter block diagram for L-LACO.

IV. Low-Complexity LACO-OFDM

A. Transmitter Design

For conventional LACO-OFDM superimposing L layers of ACO-OFDM, an $2N_{\mathrm{AC}}(l)$-point ($1 \le l \le L$) IFFT is employed in the l-th layer [23], where for readability, we define

$$N_{\mathrm{AC}}(l) = \frac{N}{2^l}. \tag{11}$$

Here we demonstrate that extending the approach of L-ACO and inspired by LAC-OFDM [20], an identical LACO-OFDM signal can be generated by using half-sized IFFTs.

In the l-th ACO-OFDM layer, $N_{\mathrm{AC}}(l)$ symbols, after considering Hermitian symmetry, are modulated onto subcarriers with index $(2p+1)2^{l-1}$ ($p = 0, 1, \ldots, N_{\mathrm{AC}}(l)$) and the remaining subcarriers are set to zero [14], resulting in the frequency domain symbol vector

$$\mathbf{Y}_{\mathrm{L}}^{(l)} = \left[0, \ldots, 0, Y_{2^{l-1}}, 0, \ldots, 0, Y_{3\cdot 2^{l-1}}, 0, \ldots, 0, Y^*_{2^{l-1}}, 0, \ldots, 0\right]. \tag{12}$$

The output of an N-point IFFT of $\mathbf{Y}_{\mathrm{L}}^{(l)}$ has a period of $2N_{\mathrm{AC}}(l)$ with an anti-symmetry inside each period [14]. Conventional LACO-OFDM generates this output signal by employing a $2N_{\mathrm{AC}}(l)$-point IFFT and repeating the frame in time-domain $2^{(l-1)}$ times.

Consider the transmitter block diagram of L-LACO in Fig. 1 where an identical LACO-OFDM frame can be generated using half-size IFFTs. Generalizing the approach of L-ACO in Section III, L-LACO constructs the anti-symmetry directly in time-domain as

$$\mathbf{y}^{(l)} = \left[\mathbf{v}^{(l)}, -\mathbf{v}^{(l)}\right] \tag{13}$$

where $\mathbf{v}^{(l)}$ is an $N_{\mathrm{AC}}(l)$-length real-valued vector with the n-th element given as

$$v_n^{(l)} = s_n^{(l)} x_n^{(l)} \tag{14}$$

where $s_n^{(l)} = \frac{1}{\sqrt{2^l}} W^{n}_{\frac{N}{2^{l-1}}}$ and

$$x_n^{(l)} = \frac{1}{\sqrt{N/2^l}} \sum_{q=0}^{\frac{N}{2^l}-1} X_q^{(l)} W_{\frac{N}{2^l}}^{nq} \tag{15}$$

and $X_q^{(l)} = Y^{(l)}_{\mathrm{L},(2q+1)2^{l-1}}$, $q = 0, 1, \ldots, N_{\mathrm{AC}}(l) - 1$, $Y^{(l)}_{\mathrm{L},(2q+1)2^{l-1}}$ is given in (12). Notice that (15) is exactly an $N_{\mathrm{AC}}(l)$-point IFFT, which indicates that a half-size IFFT can be employed in each layer to generate an identical signal to LACO-OFDM.

The negative samples of $\mathbf{y}^{(l)}$ are clipped at zero to meet the non-negativity constraint leading to $\mathbf{y}_{\mathrm{c}}^{(l)}$, denoted in Fig. 1 by the block 'Zero clipping'. Hence, the n-th ($0 \le n \le 2N_{\mathrm{AC}}(l) - 1$) element of $\mathbf{y}_{\mathrm{c}}^{(l)}$ is given as

$$y_{\mathrm{c},n}^{(l)} = \frac{1}{2} y_{\mathrm{c},n}^{(l)} + c_n^{(l)} \tag{16}$$

where $c_n^{(l)} = \frac{1}{2}|y^{(l)}_{\mathrm{mod}(n, N_{\mathrm{AC}}(l))}|$ is CD falling on the $k2^l$-th ($k = 0, 1, \ldots, N_{\mathrm{AC}}(l) - 1$) subcarriers, which is orthogonal to the data-bearing subcarriers in the l-th layer. $\mathbf{c}^{(l)}$ is a vector of length N. In each layer, $\mathbf{y}_{\mathrm{c}}^{(l)}$ is repeated 2^{l-1} times resulting in $y_{\mathrm{L},n}^{(l)}$ of length N, given by

$$\mathbf{y}_{\mathrm{L}}^{(l)} = \Bigg[\underbrace{\mathbf{y}_c^{(l)}, \ldots, \mathbf{y}_c^{(l)}}_{\text{repeat } 2^{l-1} \text{ times}}\Bigg]. \tag{17}$$

The L layers of ACO-OFDM signals are added together leading to L-LACO signal given by

$$\mathbf{z} = \sum_{l=1}^{L} \mathbf{y}_{\mathrm{L}}^{(l)}. \tag{18}$$

Thus, the L-LACO signal $\mathbf{z}$ generated using this procedure is identical to LACO-OFDM while using a half-sized IFFT in each layer resulting in fewer required operations (multiplications and additions).

The signal $\mathbf{z}$ is then converted from parallel to serial (P/S) and a cyclic prefix (CP) is appended to the front of each OFDM symbol to avoid inter-symbol interference (ISI). After a digital-to-analog converter (DAC) and a low-pass filter (LPF), the resulting analog signal $z(t)$ is utilized to drive an LED.

Figure 2 presents an example of the signals used to construct the second layer signal, $y_{\mathrm{L},n}^{(2)}$, for L-LACO where $N = 64$ and $M = 16$. Denote $x_{\mathrm{r},n}^{(2)}$ and $x_{\mathrm{i},n}^{(2)}$ as the real and imaginary parts of $x_n^{(2)}$, respectively. As shown in Fig. 2, the complex-valued output of the IFFT, $x_n^{(2)}$ is used to generate the real-valued signal, $v_n^{(2)}$ and then to construct a signal,

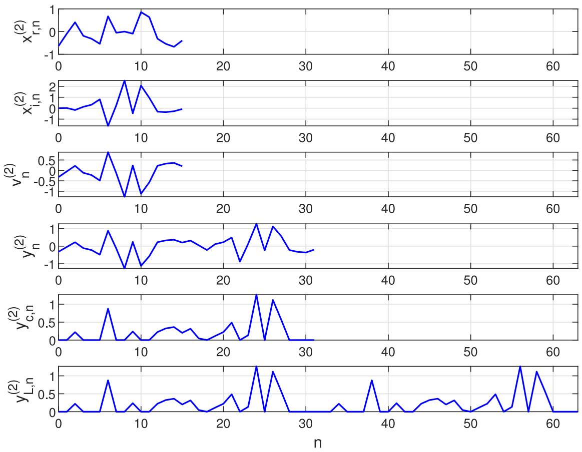

Fig. 2. An illustration of the construction of a second layer ($l = 2$) L-ACO signal, $y_{\mathrm{L},n}^{(2)}$, for L-LACO ($N = 64$ and $M = 16$).

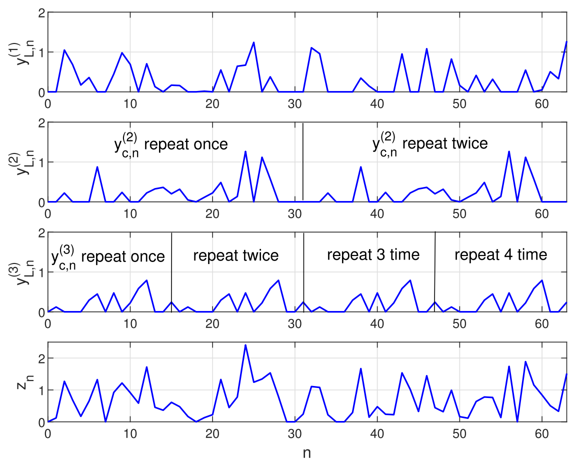

Fig. 3. An illustration of the L-LACO signals at each layer ($y_{\mathrm{L},n}^{(l)}$) and sum (z_n) ($N = 64$, $L = 3$ and $M = 16$).

$y_n^{(2)}$, with anti-symmetry imposed in time-domain. The signal $y_n^{(2)}$ is then clipped at zero leading to $y_{\mathrm{c},n}^{(2)}$, which is repeated twice resulting in the second layer signal, $y_{\mathrm{L},n}^{(2)}$.

Figure 3 shows an illustration of the construction of a complete L-LACO signal ($L = 3$, $N = 64$, $M = 16$). Notice that the first layer does not repeat while the second layer repeats two times and the third layer repeats four times. These output signals are identical to conventional LACO-OFDM, however, the size of the IFFTs used to compute each layer are half-sized.

B. Receiver Design

At the receiver side, the optical signal is first converted into an electrical current using a PD. Shot noise and thermal noise are well modelled as additive white Gaussian noise (AWGN) [7], [15], [59]. Hence, the received signal is given by

$$r(t) = h(t) * z(t) + n(t) \tag{19}$$

where $h(t)$ denotes channel impulse response, '$*$' denotes the convolution operation and $n(t)$ is the AWGN. After a low-pass filter, analog-to-digital conversion (ADC), removal of CP, and

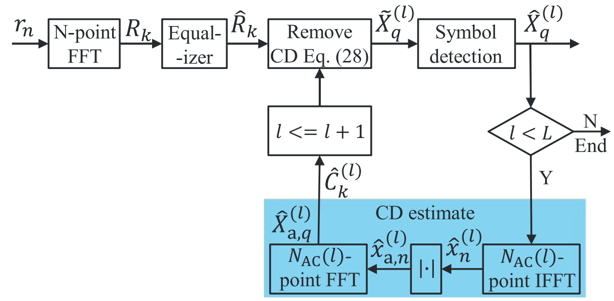

Fig. 4. Receiver block diagram for L-LACO. Note that, in contrast to the LACO-OFDM receiver in [23], L-LACO uses half-size IFFT/FFT to estimate the CD (indicated in the shaded box). The index *l* has starting value initialized to 1.

serial to parallel (P/S) conversion, the discrete received signal r_n is obtained.

Recall that the L-LACO transmitted signal **z** generated in Section IV-A is identical to LACO-OFDM though using half-size IFFT in each layer. Hence, r_n can be demodulated using a conventional LACO-OFDM receiver designed in [23], which removes CD induced by the *l*-th layer using $2N_{\mathrm{AC}}(l)$-point IFFT and $2N_{\mathrm{AC}}(l)$-point FFT.

Here a low-complexity receiver is proposed for LACO-OFDM and L-LACO, which removes CD induced by the *l*-th layer using $N_{\mathrm{AC}}(l)$-point IFFT and $N_{\mathrm{AC}}(l)$-point FFT that are half-size compared to conventional LACO-OFDM receiver. It is worth to noting that the proposed low-complexity receiver can also be used to demodulate LACO-OFDM.

Fig. 4 presents a block diagram of low-complexity receiver for L-LACO. The received signal r_n is fed into an *N*-point FFT followed by a one-tap equalizer. Since there is no CD affecting data-bearing subcarriers in the first layer, an estimate of X_q is obtained considering only the odd subcarriers

$$\widetilde{X}_q^{(1)} = 2\widehat{R}_{2q+1}, \; q = 0, 1, \ldots, N/2 - 1 \tag{20}$$

where the factor 2 is due to zero clipping operation according to (16). Due to Hermitian symmetry, only symbols in the first half of an OFDM frame are required to be detected as

$$\widehat{X}_q^{(1)} = \arg \min_{X \in \Omega_X} |\widetilde{X}_q^{(1)} - X|, \; q = 0, \; 1, \ldots, N/4 - 1 \tag{21}$$

where Ω_X denotes the constellation set.

Note that the CD from lower layers only impacts higher layers [23]. Hence, prior to detecting symbols in the second layer, CD from the first layer must be removed. The CD induced by the first layer is given by $c_n^{(1)} = \frac{1}{2}|y_n^{(1)}| = \frac{1}{2\sqrt{2}}|x_{\mathrm{mod}(n,N/2)}^{(1)}|$, according to (16) and (17), which has a period of *N*/2. Hence, the discrete Fourier tranform (DFT) of the CD induced by the first layer is given as

$$C_k^{(1)} = \frac{1}{\sqrt{N}} \sum_{n=0}^{N-1} c_n^{(1)} W_N^{-nk} \tag{22a}$$

$$= \frac{1}{2\sqrt{N}} \sum_{n=0}^{N/2-1} \left| y_n^{(1)} \right| W_N^{-nk} (1 + \cos(k\pi)) \tag{22b}$$

$$= \frac{1/2}{\sqrt{2N}} \sum_{n=0}^{N/2-1} \left|x_n^{(1)}\right| W_N^{-nk}(1+\cos(k\pi)) \tag{22c}$$

$$= \begin{cases} \frac{1}{2}\frac{1}{\sqrt{N/2}}\sum_{n=0}^{N/2-1}\left|x_n^{(1)}\right| W_N^{-nk}, & k \in \mathbb{K}_{\text{clip}}^{(1)} \\ 0, & \text{Otherwise,} \end{cases} \tag{22d}$$

$$= \begin{cases} \frac{1}{2}X_{\mathrm{a},q}^{(1)}, & k \in \mathbb{K}_{\text{clip}}^{(1)}, \ q = k/2 \\ 0, & \text{Otherwise,} \end{cases} \tag{22e}$$

where (22a) is definition of DFT and (22b) is due to clipping distortion $c_n^{(1)} = \frac{1}{2}|y_n^{(1)}|$ with a period of *N*/2, according to (16) and (17). Equation (22c) is due to $|y_n^{(1)}| = \frac{1}{\sqrt{2}}|x_{\mathrm{mod}(n,N/2)}^{(1)}|$ according to (13) and (14) with $l = 1$. In (22d), $\mathbb{K}_{\text{clip}}^{(1)} \triangleq \{k|k = 2q, \ q = 0, \ldots, N/2-1\}$. In (22e), $X_{\mathrm{a},q}^{(1)}$ is given by

$$X_{\mathrm{a},q}^{(1)} = \frac{1}{\sqrt{N/2}} \sum_{n=0}^{N/2-1} x_{\mathrm{a},n}^{(1)} W_{N/2}^{-nq} \tag{23}$$

where $x_{\mathrm{a},n}^{(1)} = |x_n^{(1)}|$ and $x_n^{(1)}$ is given by (15) with $l = 1$, which is an $\frac{N}{2}$-point IFFT. Additionally, note that (23) is an $\frac{N}{2}$-point FFT.

Hence, an estimate of the second layer can be estimated as

$$\widetilde{X}_q^{(2)} = 2\widehat{R}_{(2q+1)2} - 2\widehat{C}_{(2q+1)2}^{(1)}, \ q = 0, \ 1, \ldots, N/4-1 \tag{24}$$

where $\widehat{C}_k^{(1)}$ is an estimate of CD $C_k^{(1)}$ calculated according to (22) and replace $X_q^{(1)}$ with its estimate $\widehat{X}_q^{(1)}$. It is apparent that the factor 1/2 in (22) and 2 in (24) cancel, saving two multiplications.

Symbols in the second layer are thus detected as

$$\widehat{X}_q^{(2)} = \arg\min_{X\in\Omega_X}\left|\widetilde{X}_q^{(2)} - X\right|, \ q = 0, \ 1, \ldots, N/8-1. \tag{25}$$

More generally, according to (16) and (17), the CD induced by *l*-th ($1 \le l \le L$) layer is $c_n^{(l)} = \frac{1}{2}|y_{\mathrm{mod}(n,N/2^{l-1})}^{(l)}| = \frac{1}{2\sqrt{2^l}}|x_{\mathrm{mod}(n,N/2^l)}^{(l)}|$ with a period of $N_{\mathrm{AC}}(l)$. Hence, its DFT is given by

$$C_k^{(l)} = \frac{1}{\sqrt{N}} \sum_{n=0}^{N-1} c_n^{(l)} W_N^{-nk} \tag{26a}$$

$$= \frac{1}{2\sqrt{N}} \sum_{n=0}^{N/2^l-1} |y_n^{(l)}| W_N^{-nk} \times \left(1 + W_N^{-\frac{N}{2^l}k} + \ldots + W_N^{-(2^l-1)\frac{N}{2^l}k}\right) \tag{26b}$$

$$= \frac{1/2}{\sqrt{2^l N}} \sum_{n=0}^{N/2^l-1} \left|x_n^{(l)}\right| W_N^{-nk} \times \left(1 + W_N^{-\frac{N}{2^l}k} + \ldots + W_N^{-(2^l-1)\frac{N}{2^l}k}\right) \tag{26c}$$

$$= \begin{cases} \frac{1}{2}\frac{1}{\sqrt{N/2^l}}\sum_{n=0}^{N/2^l-1}\left|x_n^{(l)}\right| W_N^{-nk}, & k \in \mathbb{K}_{\text{clip}}^{(l)} \\ 0, & \text{Otherwise,} \end{cases} \tag{26d}$$

$$= \begin{cases} \frac{1}{2}X_{\mathrm{a},q}^{(l)}, & k \in \mathbb{K}_{\text{clip}}^{(l)}, \ q = k/2^l \\ 0, & \text{Otherwise} \end{cases} \tag{26e}$$

where (26a) is DFT definition, and (26b) is due to that the CD induced by *l*-th ($1 \le l \le L$) layer is $c_n^{(l)} = \frac{1}{2}|y_{\mathrm{mod}(n,N/2^{l-1})}^{(l)}|$ with a period of $N/2^l$. Equation (26c) is due to $|y_{\mathrm{mod}(n,N/2^{l-1})}^{(l)}| = \frac{1}{\sqrt{2^l}}|x_{\mathrm{mod}(n,N/2^l)}^{(l)}|$ according to (13) and (14). In (26d), $\mathbb{K}_{\text{clip}}^{(l)} \triangleq \{k|q2^l, \ q = 0, \ldots, N_{\mathrm{AC}}(l)-1\}$. In (26e), $X_{\mathrm{a},q}^{(l)}$ is the DFT of $x_{\mathrm{a},n}^{(l)} = |x_n^{(l)}|$, which is given by

$$X_{\mathrm{a},q}^{(l)} = \frac{1}{\sqrt{N/2^l}} \sum_{n=0}^{N/2^l-1} x_{\mathrm{a},n}^{(l)} W_{N/2^l}^{-nq} \tag{27}$$

where $x_n^{(l)}$ is calculated according to (15), which is an $N_{\mathrm{AC}}(l)$-point IFFT. As was noted for the first layer, note that (27) is an $N_{\mathrm{AC}}(l)$-point FFT.

As shown in [23], prior to demodulating ACO-OFDM symbols on the *k*-th ($k = (2q+1)2^{l-1}$) subcarrier in the *l*-th ($1 < l \le L$) layer, CD from lower layers must be removed first. Hence, we obtain an estimate for $X_q^{(l)}$ as

$$\widetilde{X}_q^{(l)} = 2\widehat{R}_{(2q+1)2^{l-1}} - 2\sum_{\eta=1}^{l-1}\widehat{C}_{(2q+1)2^{l-1}}^{(\eta)}, \quad q = 0, \ 1, \ldots, N_{\mathrm{AC}}(l)-1 \tag{28}$$

where $\widehat{C}_k^{(\eta)}$ is an estimate of CD $C_k^{(\eta)}$ calculated according to (26) replacing $X_{\mathrm{a},q}^{(\eta)}$ with its estimate $\widehat{X}_{\mathrm{a},q}^{(\eta)}$.

Thanks to the Hermitian symmetry, only symbols in the first half OFDM frame are required to be detected employing symbol detection for the *l*-th ($1 < l \le L$) layer as

$$\widehat{X}_q^{(l)} = \arg\min_{X\in\Omega_X}|\widetilde{X}_q^{(l)} - X|, \ q = 0, 1, \ldots, N_{\mathrm{AC}}(l)/2-1. \tag{29}$$

Remark 1: Compared to the LACO-OFDM receiver in [23], the proposed L-LACO receiver is less complex. In the proposed L-LACO receiver, the CD induced by *l*-th layer is estimated using single $N_{\mathrm{AC}}(l)$-point FFT and single $N_{\mathrm{AC}}(l)$-point IFFT, whereas LACO-OFDM receiver utilizes one $2N_{\mathrm{AC}}(l)$-point FFT and one $2N_{\mathrm{AC}}(l)$-point IFFT.

V. Computational Complexity Analysis

As described above, the transmitter and receiver of L-LACO require half-size IFFT/FFT compared to LACO-OFDM thus requires less computational complexity. In this section, we quantify the reduction in complexity for L-LACO over LACO-OFDM for a given set of modulation parameters.

A. Complexity Analysis of Low-Complexity ACO-OFDM

Similar to [20], we assume in the subsequent analysis that operations such as anti-symmetry construction (7) and (13) do not require any arithmetic operations since they can efficiently implement with switching logic. Additionally, the scaled twiddle factors s_n in (8) and $s_n^{(l)}$ in (14) can be precomputed and stored in a table. Furthermore, the complexity of zero clipping in (10) and (16), and symbol detection on each carrier according to (21) and (29) are not included and will be identical for both L-LACO and LACO-OFDM.

Specifically, for conventional ACO-OFDM, a single N-point IFFT and N-point FFT are required at the transmitter and the receiver, respectively. Hence, complexity can be quantified by counting the required number of real-valued multiplication operations (RMOs) and of real-valued addition operations (RAOs) for each N-point IFFT/FFT. Based on Cooley-Tukey decomposition [60], an N-point (N a power of 2) IFFT/FFT requires $M(N)$ RMOs and $A(N)$ RAOs, which are given by

$$M(N) = 2N\log_2(N) - 4N + 4 \tag{30}$$

and

$$A(N) = 3N\log_2(N) - 2N + 2. \tag{31}$$

Notice that in the L-ACO transmitter, $v_n, 0 \le n \le N/2-1$, is real according to (8). Hence RMOs between the real parts of s_n and x_n, and RMOs between the imaginary parts are necessary, i.e., only *two* RMOs and *one* RAO are required to generate v_n in (8). Considering signals with $N/2$ samples, N RMOs and $N/2$ RAOs are additionally required for v_n and thus y_n $(0 \le n \le N/2-1)$ besides the $N/2$-point IFFT in (9). Hence, the required numbers of RMOs and RAOs for L-ACO are

$$M^{(\mathrm{t})}_{\text{L-ACO}}(N) = M\left(\frac{N}{2}\right) + N = N\log_2(N) - 2N + 4 \tag{32}$$

and

$$A^{(\mathrm{t})}_{\text{L-ACO}}(N) = A\left(\frac{N}{2}\right) + \frac{N}{2} = \frac{3}{2}N\log_2(N) - 2N + 2. \tag{33}$$

At the receiver side, since L-ACO employs conventional ACO-OFDM receiver, its computational complexity is the same as ACO-OFDM.

B. Complexity Analysis of Low-Complexity LACO-OFDM

At the transmitter of L-LACO, each ACO-OFDM layer requires an $N_{\mathrm{AC}}(l)$-point IFFT. The factors $s_n^{(l)}$ in (14) can be precomputed and stored. Similar to L-ACO, it is known a priori that $v_n^{(l)}$ and $y_n^{(l)}$ are real-valued thanks to Hermitian symmetry of the input vector according to (12). Hence RMOs between the real parts of $s_n^{(l)}$ and $x_n^{(l)}$, and RMOs between their imaginary parts are necessary, i.e., only *two* RMOs and *one* RAO are required to generate $v_n^{(l)}$ in (14). Considering that the length of $\mathbf{v}^{(l)}$ is $N_{\mathrm{AC}}(l)$, $2N_{\mathrm{AC}}(l)$ RMOs and $N_{\mathrm{AC}}(l)$ RAOs are additionally required for $v_n^{(l)}$ and y_n $(0 \le n \le N_{\mathrm{AC}}(l)-1)$ besides the $N_{\mathrm{AC}}(l)$-point IFFT in (15).

Hence, the required numbers of RMOs and of RAOs for L-LACO transmitter are

$$\begin{aligned} M^{(\mathrm{t})}_{\text{L-LACO}}(L,N) &= \underbrace{\sum_{l=1}^{L} M\left(\frac{N}{2^l}\right)}_{\text{For IFFTs}} + \underbrace{\sum_{l=1}^{L} 2N_{\mathrm{AC}}(l)}_{\text{Calculate } v_n^{(l)} \text{ in (14)}} \\ &= \left(1-\frac{1}{2^L}\right)2N\log_2(N) - \left(6 - \frac{L+3}{2^{L-1}}\right)N + 4L \end{aligned} \tag{34}$$

and

$$\begin{aligned} A^{(\mathrm{t})}_{\text{L-LACO}}(L,N) &= \underbrace{\sum_{l=1}^{L} A\left(\frac{N}{2^l}\right)}_{\text{For IFFTs}} + \underbrace{(L-1)N}_{\text{SumLlayers}} + \underbrace{\sum_{l=1}^{L} N_{\mathrm{AC}}(l)}_{\text{Calculate } v_n^{(l)} \text{ in (14)}} \\ &= \left(1-\frac{1}{2^L}\right)3N\log_2(N) \\ &\quad - \left(8 - L - \frac{3L+7}{2^L}\right)N + 2L. \end{aligned} \tag{35}$$

At the receiver side of L-LACO as shown in Fig. 4, the N-point FFT requires $M(N)$ RMOs and $A(N)$ RAOs. When a one-tap zero-forcing equalizer (ZFE) is adopted, it requires $N/2$ complex-valued multiplications or $2N$ RMOs and N RAOs thanks to the Hermitian symmetry. It is apparent that the computational complexity induced by a ZFE is also required by LACO-OFDM. Additionally, the estimate of CD requires a single $N_{\mathrm{AC}}(l)$-point IFFT and a single $N_{\mathrm{AC}}(l)$-point FFT for l-th $(1 \le l \le L-1)$ layer.[1] Hence, the required numbers of RMOs and RAOs for L-LACO receiver are

$$\begin{aligned} M^{(\mathrm{r})}_{\text{L-LACO}}(L,N) &= M(N) + \underbrace{2N}_{\text{For ZFE}} + \underbrace{2\sum_{l=1}^{L-1} M\left(\frac{N}{2^l}\right)}_{\text{Estimate CD}} \\ &= \left(6 - \frac{8}{2^L}\right)N\log_2(N) \\ &\quad - \left(18 - \frac{L+3}{2^{L-3}}\right)N + 8L - 4 \end{aligned} \tag{36}$$

and

$$\begin{aligned} A^{(\mathrm{r})}_{\text{L-LACO}}(L,N) &= A(N) + \underbrace{N}_{\text{For ZFE}} + \underbrace{2\sum_{l=1}^{L-1} A\left(\frac{N}{2^l}\right)}_{\text{Estimate CD}} \\ &\quad + \underbrace{\sum_{l=2}^{L}(l-1)\frac{N}{2^l}}_{\text{Remove CD}} \\ &= \left(9 - \frac{12}{2^L}\right)N\log_2(N) \\ &\quad - \left(16 - \frac{11L+19}{2^L}\right)N + 4L - 2. \end{aligned} \tag{37}$$

For comparison, the required numbers of RMOs and RAOs for LACO-OFDM transmitter are [14], [20]

$$\begin{aligned} M^{(\mathrm{t})}_{\text{LACO}}(L,N) &= \left(1-\frac{1}{2^L}\right)4N\log_2(N) \\ &\quad - \left(12 - \frac{2L+6}{2^{L-1}}\right)N + 4L \end{aligned} \tag{38}$$

and

$$\begin{aligned} A^{(\mathrm{t})}_{\text{LACO}}(L,N) &= \left(1-\frac{1}{2^L}\right)6N\log_2(N) \\ &\quad - \left(11 - L - \frac{3L+5}{2^{L-1}}\right)N + 2L. \end{aligned} \tag{39}$$

[1]Note that the absolute value operation for real-valued numbers requires simple logic operation which is omitted in the complexity analysis.

For LACO-OFDM receiver, an identical ZFE is adopted. Hence, the required number of RMOs and RAOs for LACO-OFDM receiver are, respectively, given as [20]

$$M^{(\mathrm{r})}_{\mathrm{LACO}}(L,N) = \left(1-\frac{\frac{8}{5}}{2^L}\right)10N\log_2(N) - \left(26-\frac{L+2}{2^{L-4}}\right)N+8L-4 \quad (40)$$

and

$$A^{(\mathrm{r})}_{\mathrm{LACO}}(L,N) = \left(1-\frac{\frac{8}{5}}{2^L}\right)15N\log_2(N) - \left(19-\frac{23L+13}{2^L}\right)N+4L-2. \quad (41)$$

C. Power Savings

VLC transmitters are constrained by complexity, i.e., transmitters must be simple and integrated into inexpensive luminaires, using low cost commercially available LEDs. Additionally, VLC transmitters must be energy efficient given that the energy efficiency of LED luminaries is a primary advantage of this illumination technology. Hence, in this section, the saved power of L-LACO over LACO-OFDM is quantified due to the reduction in number of arithmetic operations.

Following the computational complexity analysis in Section V-B, the reduction in RMOs and RAOs of L-LACO transmitter over LACO-OFDM for an OFDM symbol are given as

$$\Delta^{(\mathrm{t})}_{\mathrm{Mul}} = M^{(\mathrm{t})}_{\mathrm{LACO}}(L,N) - M^{(\mathrm{t})}_{\text{L-LACO}}(L,N) \quad (42)$$

and

$$\Delta^{(\mathrm{t})}_{\mathrm{Add}} = A^{(\mathrm{t})}_{\mathrm{LACO}}(L,N) - A^{(\mathrm{t})}_{\text{L-LACO}}(L,N), \quad (43)$$

respectively.

Let the energy consumed by a single RMO and a single RAO be denoted as E_{Mul} and E_{Add}, respectively. Then the saved energy of L-LACO transmitter over LACO-OFDM for an OFDM symbol can be computed as

$$\Delta^{(\mathrm{t})}_{\mathrm{Energy}} = \Delta^{(\mathrm{t})}_{\mathrm{Mul}}E_{\mathrm{Mul}} + \Delta^{(\mathrm{t})}_{\mathrm{Add}}E_{\mathrm{Add}}. \quad (44)$$

Assume the time length of an OFDM symbol is T_{s} and the time length of CP is T_{CP}. Hence, the saved power of the L-LACO transmitter over LACO-OFDM is

$$P^{(\mathrm{t})}_{\mathrm{save}}(L,N,B) = \frac{\Delta^{(\mathrm{t})}_{\mathrm{Energy}}}{T_{\mathrm{s}}+T_{\mathrm{CP}}}. \quad (45)$$

For readability, assume $T_{\mathrm{CP}} = \beta T_{\mathrm{s}}$ without loss of generality and assume a modulation bandwidth of the VLC system is B Hz. Then the length of an OFDM frame is $T_{\mathrm{s}} = N/(2B)$ and $T_{\mathrm{s}} + T_{\mathrm{CP}} = (1+\beta)N/(2B)$. Substituting (34), (35), (38), (39), (42), (43) and (44) into (45) results in

$$P^{(\mathrm{t})}_{\mathrm{save}}(L,N,B) = \frac{2B}{1+\beta}(\gamma\log_2 N - \zeta) \quad (46)$$

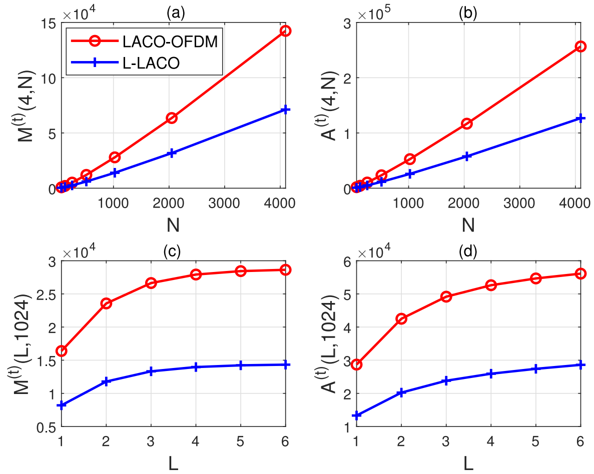

Fig. 5. Computational complexity comparison between transmitters of L-LACO and LACO-OFDM for different values of N and L ($L = 4$ for (a) and (b), $N = 1024$ for (c) and (d)).

where $\gamma \triangleq (1-1/2^L)(2E_{\mathrm{Mul}}+3E_{\mathrm{Add}})$ and $\zeta \triangleq (6-\frac{L+3}{2^{L-1}})E_{\mathrm{Mul}} + (3-\frac{3L+3}{2^L})E_{\mathrm{Add}}$.

Using a similar approach, the saved power of L-LACO receiver over existing LACO-OFDM can be calculated as

$$P^{(\mathrm{r})}_{\mathrm{save}}(L,N,B) = \frac{\Delta^{(\mathrm{r})}_{\mathrm{Energy}}}{T_{\mathrm{s}}+T_{\mathrm{CP}}} \quad (47)$$

where $\Delta^{(\mathrm{r})}_{\mathrm{Energy}} = \Delta^{(\mathrm{r})}_{\mathrm{Mul}}E_{\mathrm{Mul}} + \Delta^{(\mathrm{r})}_{\mathrm{Add}}E_{\mathrm{Add}}$ is saved energy of L-LACO receiver for an OFDM symbol while $\Delta^{(\mathrm{r})}_{\mathrm{Mul}} = M^{(\mathrm{r})}_{\mathrm{LACO}}(L,N) - M^{(\mathrm{r})}_{\text{L-LACO}}(L,N)$ denotes saved RMOs and $\Delta^{(\mathrm{r})}_{\mathrm{Add}} = A^{(\mathrm{r})}_{\mathrm{LACO}}(L,N) - A^{(\mathrm{r})}_{\text{L-LACO}}(L,N)$ denotes saved RAOs, respectively.

Substituting (36), (37), (40) and (41) into (47) gives

$$P^{(\mathrm{r})}_{\mathrm{save}}(L,N,B) = \frac{2B}{1+\beta}(\psi\log_2 N - \xi) \quad (48)$$

where $\psi \triangleq (1-2/2^L)(4E_{\mathrm{Mul}}+6E_{\mathrm{Add}})$ and $\xi \triangleq (8-\frac{L+1}{2^{L-3}})E_{\mathrm{Mul}} + (3-\frac{6L-3}{2^{L-1}})E_{\mathrm{Add}}$.

Remark 2: As L increases with B and N fixed, γ and ζ in (46), ψ and ξ in (48) saturate to a constant, respectively as do $P^{(\mathrm{t})}_{\mathrm{save}}(L,N,B)$ and $P^{(\mathrm{r})}_{\mathrm{save}}(L,N,B)$. As N increases with B and L fixed, $P^{(\mathrm{t})}_{\mathrm{save}}(L,N,B)$ increases logarithmically as does $P^{(\mathrm{r})}_{\mathrm{save}}(L,N,B)$. As B increases with L and N fixed, both $P^{(\mathrm{t})}_{\mathrm{save}}(L,N,B)$ and $P^{(\mathrm{r})}_{\mathrm{save}}(L,N,B)$ increase linearly.

VI. Numerical Results

A. Computational Complexity

Numerical results for the computational complexity of L-LACO are presented and compared to LACO-OFDM [23] with realistic parameters for VLC systems.

A computational complexity comparison between transmitters of L-LACO and LACO-OFDM for different values of N and L are shown in Fig. 5, in which for (a) and (b) L is fixed to 4 while for (c) and (d) N is fixed to 1024. It is evident that the conventional LACO-OFDM is more complex than our proposed L-LACO in terms of the number of

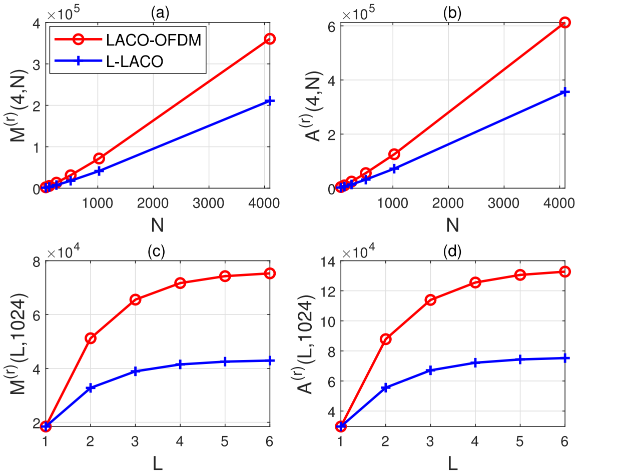

Fig. 6. Computational complexity comparison between receivers of L-LACO and LACO-OFDM for different values of N and L ($L = 4$ for (a) and (b), $N = 1024$ for (c) and (d)).

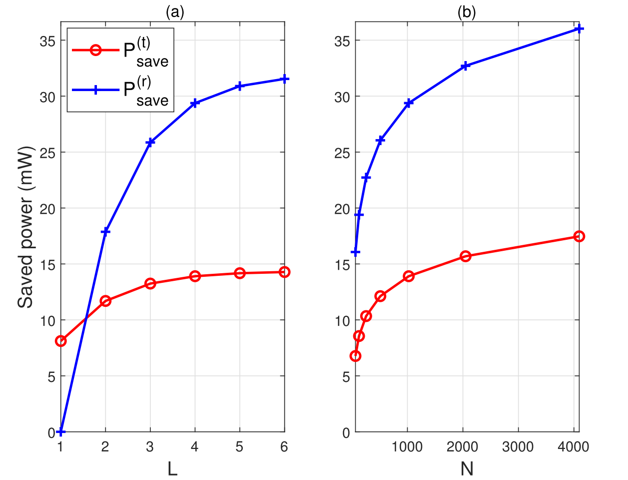

Fig. 7. Power saving of L-LACO compared to LACO-OFDM for different values of L and N when $B = 100$ MHz ($N = 1024$ for (a) and $L = 4$ for (b)).

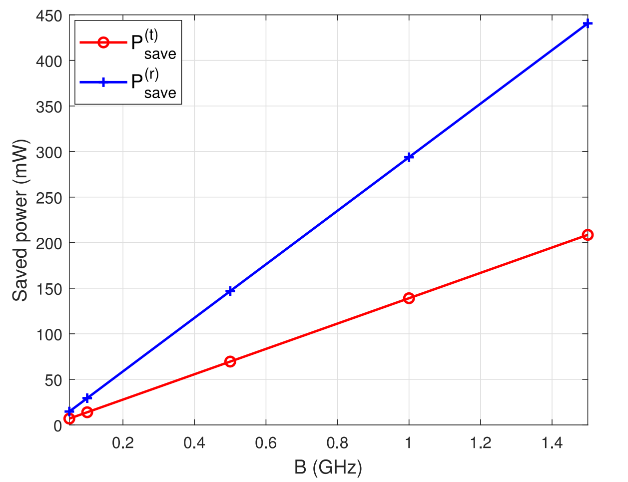

Fig. 8. Saved power of L-LACO compared to LACO-OFDM for different values of B ($L = 4$ and $N = 1024$).

RMOs and RAOs. More specifically, for $L = 4$ layers and $N = 1024$ subcarriers, LACO-OFDM requires 27920 RMOs and 52620 RAOs; while our proposed L-LACO requires 13970 RMOs and 25930 RAOs. LACO-OFDM requires two times more RMOs/RAOs when compared with our proposed L-LACO.

For receivers, a computational complexity comparison between L-LACO and LACO-OFDM for different values of N and L are shown in Fig. 6, in which for (a) and (b) L is fixed to 4 while for (c) and (d) N is fixed to 1024. Evidently, the LACO-OFDM receiver is more complex than our proposed L-LACO in terms of the number of RMOs and RAOs since the size of IFFT/FFT used to remove CD induced by each layer are halved in L-LACO. Specifically, LACO-OFDM requires 71710 RMOs and 125518 RAOs when $L = 4$ and $N = 1024$; while our proposed low-complexity L-LACO requires 41500 RMOs and 72142 RAOs. LACO-OFDM requires nearly 1.73 times more RMOs and 1.74 times more RAOs when compared with our proposed L-LACO.

The number of RMOs and RAOs of both L-LACO transmitter and receiver increase dramatically fast as N increases. This is because the dominant term of $M^{(\mathrm{t})}_{\text{L-LACO}}(L,N)$, $A^{(\mathrm{t})}_{\text{L-LACO}}(L,N)$, $M^{(\mathrm{r})}_{\text{L-LACO}}(L,N)$, and $A^{(\mathrm{r})}_{\text{L-LACO}}(L,N)$ are respectively $(1-1/2^L)2N\log_2(N)$, $(1-1/2^L)3N\log_2(N)$, $(6-8/2^L)N\log_2(N)$ and $(9-12/2^L)N\log_2(N)$, which increase faster than linear functions of N when N is large. While the number of RMOs and RAOs increase more slowly and saturate as L increases when $N = 1024$. This is because the previously noted dominant terms, for a fixed N, saturate to limit with increasing L.

B. Saved Power

According to [61], a 32-bit floating point multiplication and a 32-bit floating point addition consume $E_{\text{Mul}} = 3.7$ pJ and $E_{\text{Add}} = 0.9$ pJ, respectively. Assume a modulation bandwidth of $B = 100$ MHz and that the length of an OFDM frame is $T_{\mathrm{s}} = N/(2B)$ and $T_{\mathrm{CP}} = T_{\mathrm{s}}/16$ with $\beta = 1/16$.

The saved power of L-LACO over LACO-OFDM is then calculated according to Section V-C and presented for different values of L and N in Fig. 7. It can be seen the saved power of L-LACO receiver is higher than L-LACO transmitter when $L \geq 2$, which is aligned well given that the L-LACO receiver saved more arithmetic operations than L-LACO transmitter shown in Figs. 5 and 6. In addition, compared to LACO-OFDM, the saved power of L-LACO transmitter and receiver increase and saturate as L increases when $N = 1024$, which is aligned well with theoretical analysis in Section V-C and Remark 2. This is because the saved arithmetic operations increase and saturate as L increases.

In contrast, notice that the saved power of the L-LACO transmitter over LACO-OFDM increases logarithmically with N as does the saved power of the L-LACO receiver. This trend agrees well with theoretical analysis in Remark 2.

The saved power of the L-LACO transmitter and receiver over LACO-OFDM for different values of modulation bandwidth is shown in Fig. 8. The saved power of the L-LACO transmitter and receiver increase linearly as modulation bandwidth B increases when $L = 4$ and $N = 1024$. This is

TABLE IV
SIMULATION PARAMETERS

Parameters	Values
Room size Width × Length × Height	5m × 5m × 3m
Number of LED/PD	1 / 1
LED location	(2.5, 2.5, 2.50) m
LED semi-angle $\Psi_{1/2}$	45^o
PD location	(2.5, 2.5, 0.75) m
Optical power gain of receive filter	1
PD FOV Θ_{F}	62^o [65]
PD effective collection area A_{PD}	1 cm^2
O/E conversion coefficient η	0.54 A/W [66]
Average electrical noise power σ_w^2	-98.82 dBm [66]
Number of subcarriers N	1024
Number of layers L	3
Length of CP N_{CP}	64
Maximum delay spread $D_{\max}$	64
Modulation schemes	4-QAM, 16-QAM

aligned well with theoretical analysis in Remark 2. Notice that the power savings become especially significant for high-speed VLC systems realized using L-LACO.

It is worth noting that the saved power will increase linearly for larger B. For example, $B = 600$ MHz for Si-substrate LED [62], $B = 655$ MHz for micro-LED [63] and $B = 1.4$ GHz for laser diode (LD) based white-light VLC [64] are reported in recent experimental demonstrations. Thus, L-LACO becomes an even more attractive approach with the arrival of new high-bandwidth light sources envisioned for future VLC applications.

C. BER Performance

In this section, the BER performance of L-LACO is evaluated by back-to-back simulations in terms of transmitted optical power P_{o} expressed in decibel milliwatts (dBm), and compared with LACO-OFDM. Assume $B = 100$ MHz.

1) BER Under a VLC LOS Link: The BER of L-LACO under a VLC LOS Link is simulated with parameters summarized in Table IV.

The BER performance of the proposed L-LACO and of LACO-OFDM under a VLC LOS link is shown in Fig. 9, where 4-QAM and 16-QAM with Gray labelling are employed in each layer. The BER of each layer are approximately the samen when operating in the high SNR regime. In addition, the BER of the proposed L-LACO is the same as existing LACO-OFDM since L-LACO generates the same OFDM symbol as LACO-OFDM, however, L-LACO requires less complexity at both the transmitter and the receiver thanks to employing half-size IFFTs/FFTs.

2) BER Under a VLC Dispersive Channel: In this section, the BER of L-LACO under a VLC dispersive channel is simulated. Here, the sampling rate for impulse response $h(t)$ in (2) is set to 300 MHz. The maximum delay span of samples of $h(t)$ is assumed to 64. Hence, the length of CP is also set to $N_{\mathrm{CP}} = 64$.

The BER performance of the proposed L-LACO and of LACO-OFDM under a VLC dispersive channel are shown in Fig. 10, where the simulation parameters are summarized in Table IV. The BER of each layer in these Monte Carlo simulations are in close agreement especially at high SNR.

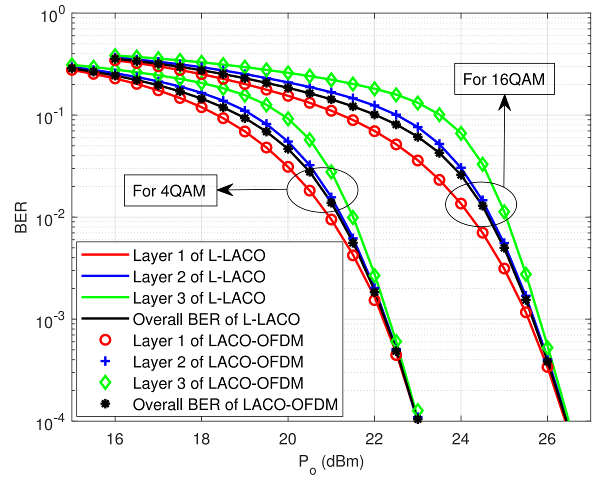

Fig. 9. BER performance of L-LACO and LACO-OFDM under a VLC LOS channel.

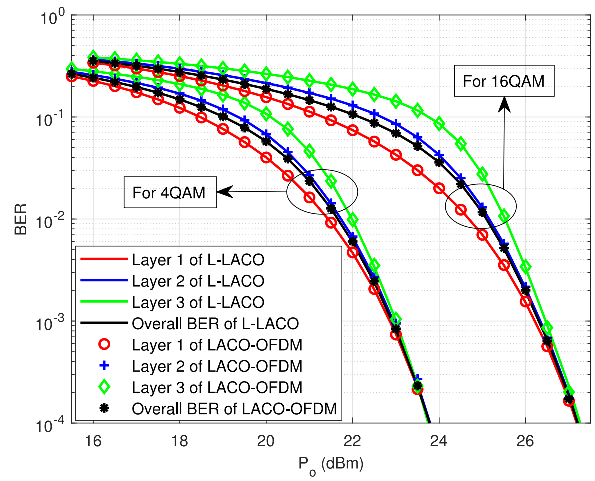

Fig. 10. BER performance of L-LACO and LACO-OFDM under a VLC dispersive channel.

Additionally, the BER of the proposed L-LACO is the same as LACO-OFDM since L-LACO generates identical signal to LACO-OFDM, however, L-LACO requires less complexity at both the transmitter and the receiver thanks to employing a half-size IFFT/FFT.

VII. CONCLUSION

In this paper, L-LACO is proposed for IM/DD systems, in which the size of IFFT and FFT used in each layer is halved compared to the existing LACO-OFDM. The proposed L-LACO generates the identical OFDM signal to LACO-OFDM and thus achieves the same spectral efficiency and optical power efficiency but retains less complexity. Numerical results show that LACO-OFDM requires two times the RMOs/RAOs as compared to the proposed L-LACO at the transmitter. At the receiver, LACO-OFDM requires 1.73 times more RMOs and 1.74 times more RAOs when compared with the proposed L-LACO. This reduction in complexity translates directly into power savings which are especially important for LED luminaires. Additionally, the proposed L-LACO achieves the same BER performance under VLC LOS and dispersive channels thanks to the identical OFDM signals generated as LACO-OFDM.

As the bandwidth of VLC systems increases with new devices, the need for low complexity, power efficient approaches, such as L-LACO, to implement spectrally efficient IM/DD modulation becomes essential. Our future work includes experimental demonstration of L-LACO including quantifying the impact of oversampling at the transmitter and receiver.

REFERENCES

[1] L. Hanzo, H. Haas, S. Imre, D. O'Brien, M. Rupp, and L. Gyongyosi, "Wireless myths, realities, and futures: From 3G/4G to optical and quantum wireless," *Proc. IEEE*, vol. 100, pp. 1853–1888, May 2012, doi: 10.1109/JPROC.2012.2189788.

[2] P. H. Pathak, X. Feng, P. Hu, and P. Mohapatra, "Visible light communication, networking, and sensing: A survey, potential and challenges," *IEEE Commun. Surveys Tuts.*, vol. 17, no. 4, pp. 2047–2077, 4th Quart., 2015.

[3] H. Haas, J. Elmirghani, and I. White "Optical wireless communication," *Phil. Trans. Roy. Soc. A*, vol. 378, Apr. 2020, Art. no. 20200051.

[4] Z. Zhang, A. Chaaban, and M.-S. Alouini, "Residual clipping noise in multi-layer optical OFDM: Modeling, analysis, and applications," *IEEE Trans. Wireless Commun.*, vol. 19, no. 9, pp. 5846–5859, Sep. 2020.

[5] S. Hranilovic, *Wireless Optical Communication Systems*. New York, NY, USA: Springer, 2004.

[6] Z. Ghassemlooy, W. Popoola, and S. Rajbhandari, *Optical Wireless Communications: System and Channel Modelling With MATLAB®*. Milton, ON, Canada: CRC Press, 2019.

[7] J. M. Kahn and J. R. Barry, "Wireless infrared communications," *Proc. IEEE*, vol. 85, no. 2, pp. 265–298, Feb. 1997.

[8] R. Zhang and L. Hanzo, "Multi-layer modulation for intensity-modulated direct-detection optical OFDM," *J. Opt. Commun. Netw.*, vol. 5, no. 12, pp. 1402–1412, Dec. 2013.

[9] X. Zhang, Q. Wang, R. Zhang, S. Chen, and L. Hanzo, "Performance analysis of layered ACO-OFDM," *IEEE Access*, vol. 5, pp. 18366–18381, 2017.

[10] A. M. Khalid, G. Cossu, R. Corsini, P. Choudhury, and E. Ciaramella, "1-Gb/s transmission over a phosphorescent white LED by using rate-adaptive discrete multitone modulation," *IEEE Photon. J.*, vol. 4, no. 5, pp. 1465–1473, Oct. 2012.

[11] B. Ranjha and M. Kavehrad, "Hybrid asymmetrically clipped OFDM-based IM/DD optical wireless system," *J. Opt. Commun. Netw.*, vol. 6, no. 4, pp. 387–396, Apr. 2014.

[12] R. Bai, Q. Wang, and Z. Wang, "Asymmetrically clipped absolute value optical OFDM for intensity-modulated direct-detection systems," *J. Lightw. Technol.*, vol. 35, no. 17, pp. 3680–3691, Sep. 1, 2017.

[13] J. Armstrong, "OFDM for optical communications," *J. Lightw. Technol.*, vol. 27, no. 3, pp. 189–204, Feb. 1, 2009.

[14] R. Bai and S. Hranilovic, "Absolute value layered ACO-OFDM for intensity-modulated optical wireless channels," *IEEE Trans. Commun.*, vol. 68, no. 11, pp. 7098–7110, Nov. 2020.

[15] S. D. Dissanayake and J. Armstrong, "Comparison of ACO-OFDM, DCO-OFDM and ADO-OFDM in IM/DD systems," *J. Lightw. Technol.*, vol. 31, no. 7, pp. 1063–1072, Apr. 1, 2013.

[16] J. Armstrong and A. J. Lowery, "Power efficient optical OFDM," *Electron. Lett.*, vol. 42, no. 6, pp. 370–372, Mar. 2006.

[17] S. C. J. Lee, S. Randel, F. Breyer, and A. M. J. Koonen, "PAM-DMT for intensity-modulated and direct-detection optical communication systems," *IEEE Photon. Technol. Lett.*, vol. 21, no. 23, pp. 1749–1751, Dec. 1, 2009.

[18] D. Tsonev, S. Videv, and H. Haas, "Unlocking spectral efficiency in intensity modulation and direct detection systems," *IEEE J. Sel. Areas Commun.*, vol. 33, no. 9, pp. 1758–1770, Sep. 2015.

[19] N. Fernando, Y. Hong, and E. Viterbo, "Flip-OFDM for unipolar communication systems," *IEEE Trans. Commun.*, vol. 60, no. 12, pp. 3726–3733, Dec. 2012.

[20] R. Bai and S. Hranilovic, "Layered antisymmetry-constructed clipped optical OFDM for low-complexity VLC systems," *Opt. Exp.*, vol. 29, no. 7, pp. 10613–10630, Mar. 2021.

[21] M. S. Islim, D. Tsonev, and H. Haas, "On the superposition modulation for OFDM-based optical wireless communication," in *Proc. IEEE Global Conf. Signal Inf. Process. (GlobalSIP)*, Orlando, FL, USA, 2015, pp. 1022–1026.

[22] H. Elgala and T. D. C. Little, "SEE-OFDM: Spectral and energy efficient OFDM for optical IM/DD systems," in *Proc. IEEE 25th Annu. Int. Symp. Pers. Indoor Mobile Radio Commun. (PIMRC)*, Washington, DC, USA, 2014, pp. 851–855.

[23] Q. Wang, C. Qian, X. Guo, Z. Wang, D. G. Cunningham, and I. H. White, "Layered ACO-OFDM for intensity-modulated direct-detection optical wireless transmission," *Opt. Exp.*, vol. 23, no. 9, pp. 12382–12393, May 2015.

[24] A. J. Lowery, "Enhanced asymmetrically clipped optical ODFM for high spectral efficiency and sensitivity," in *Proc. IEEE Opt. Fiber Commun. Conf. Exhibit. (OFC)*, Anaheim, CA, USA, 2016, pp. 1–3.

[25] Q. Wang, Z. Wang, X. Guo, and L. Dai, "Improved receiver design for layered ACO-OFDM in optical wireless communications," *IEEE Photon. Technol. Lett.*, vol. 28, no. 3, pp. 319–322, Feb. 1, 2016.

[26] M. M. A. Mohammed, C. He, and J. Armstrong, "Diversity combining in layered asymmetrically clipped optical OFDM," *J. Lightw. Technol.*, vol. 35, no. 11, pp. 2078–2085, Jun. 1, 2017.

[27] T. Q. Wang, H. Li, and X. Huang, "Diversity combining for layered asymmetrically clipped optical OFDM using soft successive interference cancellation," *IEEE Commun. Lett.*, vol. 21, no. 6, pp. 1309–1312, Jun. 2017.

[28] T. Q. Wang, H. Li, and X. Huang, "Interference cancellation for layered asymmetrically clipped optical OFDM with application to optical receiver design," *J. Lightw. Technol.*, vol. 36, no. 11, pp. 2100–2113, Jun. 1, 2018.

[29] T. Q. Wang, H. Li, and X. Huang, "Analysis and mitigation of clipping noise in layered ACO-OFDM based visible light communication systems," *IEEE Trans. Commun.*, vol. 67, no. 1, pp. 564–577, Jan. 2019.

[30] J. Zhou *et al.*, "Low-PAPR layered/enhanced ACO-SCFDM for optical-wireless communications," *IEEE Photon. Technol. Lett.*, vol. 30, no. 2, pp. 165–168, Jan. 15, 2018.

[31] R. Bai, Z. Wang, R. Jiang, and J. Cheng, "Interleaved DFT-spread Layered/Enhanced ACO-OFDM for intensity-modulated direct-detection systems," *J. Lightw. Technol.*, vol. 36, no. 20, pp. 4713–4722, Oct. 15, 2018.

[32] W. Hu, "Design of a cyclic shifted LACO-OFDM for optical wireless communication," *IEEE Access*, vol. 8, pp. 76708–76714, 2020.

[33] F. Yang, Y. Sun, and J. Gao, "Adaptive LACO-OFDM with variable layer for visible light communication," *IEEE Photon. J.*, vol. 9, no. 6, pp. 1–8, Dec. 2017.

[34] J. Zhou and W. Zhang, "A comparative study of unipolar OFDM schemes in Gaussian optical intensity channel," *IEEE Trans. Commun.*, vol. 66, no. 4, pp. 1549–1564, Apr. 2018.

[35] X. Zhang, S. Chen, and L. Hanzo, "On the discrete-input continuous-output memoryless channel capacity of layered ACO-OFDM," *J. Lightw. Technol.*, vol. 38, no. 18, pp. 4955–4968, Sep. 15, 2020.

[36] B. Song, B. Corcoran, Q. Wang, L. Zhuang, and A. J. Lowery, "Subcarrier pairwise coding for short-haul L/E-ACO-OFDM," *IEEE Photon. Technol. Lett.*, vol. 29, no. 18, pp. 1584–1587, Sep. 15, 2017.

[37] X. Zhang, Z. Babar, S. Chen, and L. Hanzo, "Multi-class coded layered asymmetrically clipped optical OFDM," *IEEE Trans. Commun.*, vol. 67, no. 1, pp. 578–589, Jan. 2019.

[38] Z. Babar *et al.*, "Near-capacity multilayered code design for LACO-OFDM-aided optical wireless systems," *IEEE Trans. Veh. Technol.*, vol. 68, no. 4, pp. 4051–4054, Apr. 2019.

[39] C. Lacava, Z. Babar, X. Zhang, I. Demirtzioglou, P. Petropoulos, and L. Hanzo, "High-speed multi-layer coded adaptive LACO-OFDM and its experimental verification," *OSA Continuum*, vol. 3, pp. 2614–2629, Sep. 2020.

[40] Q. Wang, Z. Wang, L. Dai, and J. Quan, "Dimmable visible light communications based on multilayer ACO-OFDM," *IEEE Photon. J.*, vol. 8, no. 3, pp. 1–11, Jun. 2016.

[41] T. Wang, F. Yang, L. Cheng, and J. Song, "Spectral-efficient generalized spatial modulation based hybrid dimming scheme with LACO-OFDM in VLC," *IEEE Access*, vol. 6, pp. 41153–41162, 2018.

[42] T. Zhang, Y. Qiao, J. Zhou, Z. Zhang, Y. Lu, and F. Su, "Spectral-efficient L/E-ACO-SCFDM-based dimmable visible light communication system," *IEEE Access*, vol. 7, pp. 10617–10626, 2019.

[43] B. Li, W. Xu, S. Feng, and Z. Li, "Spectral-efficient reconstructed LACO-OFDM transmission for dimming compatible visible light communications," *IEEE Photon. J.*, vol. 11, no. 1, pp. 1–14, Feb. 2019.

[44] R. Bai and S. Hranilovic, "Absolute value layered ACO-OFDM for intensity-modulated optical wireless channels," in *Proc. IEEE Int. Conf. Commun. (ICC)*, Shanghai, China, 2019, pp. 1–6.

[45] T. Zhang, H. Ji, Z. Ghassemlooy, X. Tang, B. Lin, and S. Qiao, "Spectrum-efficient triple-layer hybrid optical OFDM for IM/DD-based optical wireless communications," *IEEE Access*, vol. 8, pp. 10352–10362, 2020.

[46] S. Feng, R. Zhang, W. Xu, and L. Hanzo, "Multiple access design for ultra-dense VLC networks: Orthogonal vs non-orthogonal," *IEEE Trans. Commun.*, vol. 67, no. 3, pp. 2218–2232, Mar. 2019.

[47] H. Li, Z. Huang, Y. Xiao, S. Zhan, and Y. Ji, "A power and spectrum efficient NOMA scheme for VLC network based on hierarchical pre-distorted LACO-OFDM," *IEEE Access*, vol. 7, pp. 48565–48571, 2019.

[48] X. Huang, F. Yang, C. Pan, and J. Song, "Flexible NOMA-based NOHO-OFDM scheme for visible light communication with iterative interference cancellation," *Opt. Exp.*, vol. 29, no. 4, pp. 5645–5657, Feb. 2021.

[49] Q. Wang *et al.*, "Hardware-efficient signal generation of layered/enhanced ACO-OFDM for short-haul fiber-optic links," *Opt. Exp.*, vol. 25, no. 12, pp. 13359–13371, Jun. 2017.

[50] Z. Zhang *et al.*, "Worst-case residual clipping noise power model for bit loading in LACO-OFDM," in *Proc. Global LIFI Congr. (GLC)*, Paris, France, 2018, pp. 1–6.

[51] B. Song, C. Zhu, B. Corcoran, Q. Wang, L. Zhuang, and A. J. Lowery, "Experimental layered/enhanced ACO-OFDM short-haul optical fiber link," *IEEE Photon. Technol. Lett.*, vol. 28, no. 24, pp. 2815–2818, Dec. 15, 2016.

[52] X. Liu, J. Li, J. Li, and Z. Huang, "Analysis of the single-FFT receiver for layered ACO-OFDM in visible light communications," *J. Lightw. Technol.*, vol. 38, no. 17, pp. 4757–4764, Sep. 1, 2020.

[53] R. Bai and S. Hranilovic, "Layered antisymmetry-constructed clipped optical OFDM for IM/DD systems," in *Proc. IEEE Global Commun. Conf. (GLOBECOM)*, Waikoloa, HI, USA, Dec. 2019, pp. 1–6.

[54] R. Bai and S. Hranilovic, "Kramers-Kronig optical OFDM for bandlimited intensity modulated visible light communications," *J. Lightw. Technol.*, vol. 39, no. 22, pp. 7135–7145, Nov. 15, 2021.

[55] S. Mazahir, A. Chaaban, H. Elgala, and M.-S. Alouini, "Achievable rates of multi-carrier modulation schemes for bandlimited IM/DD systems," *IEEE Trans. Wireless Commun.*, vol. 18, no. 3, pp. 1957–1973, Mar. 2019.

[56] A. J. Lowery, "Spectrally efficient optical orthogonal frequency division multiplexing," *Phil. Trans. Roy. Soc. A*, vol. 378, Apr. 2020, Art. no. 20190180.

[57] J. B. Carruthers and J. M. Kahn, "Modeling of nondirected wireless infrared channels," *IEEE Trans. Commun.*, vol. 45, no. 10, pp. 1260–1268, Oct. 1997.

[58] A. V. Oppenheim and R. W. Schafer, *Discrete-Time Signal Processing*, 3rd ed. Upper Saddle River, NJ, USA: Prentice-Hall Press, 2010.

[59] M.-A. Khalighi, S. Long, S. Bourennane, and Z. Ghassemlooy, "PAM- and CAP-based transmission schemes for visible-light communications," *IEEE Access*, vol. 5, pp. 27002–27013, 2017.

[60] B. Porat, *A Course in Digital Signal Processing*. New York, NY, USA: Wiley, 1997.

[61] M. Horowitz, "1.1 Computing's energy problem (and what we can do about it)," in *Int. Solid-State Circuits Conf. Dig. Tech. Papers(ISSCC)*, San Francisco, CA, USA, 2014, pp. 1–4.

[62] F. Hu *et al.*, "Si-substrate LEDs with multiple superlattice interlayers for beyond 24 Gbps visible light communication," *Photon. Res.*, vol. 9, no. 8, pp. 1581–1591, Aug. 2021.

[63] M. S. Islim *et al.*, "Towards 10 Gb/s orthogonal frequency division multiplexing-based visible light communication using a GaN violet micro-LED," *Photon. Res.*, vol. 5, no. 2, pp. A35–A43, Apr. 2017.

[64] H. Chun, A. Gomez, C. Quintana, W. Zhang, G. Faulkner, and D. O'Brien, "A wide-area coverage 35 Gb/s visible light communications link for indoor wireless applications," *Sci. Rep.*, vol. 9, no. 1, pp. 1–8, 2019.

[65] L. Zeng *et al.*, "High data rate multiple input multiple output (MIMO) optical wireless communications using white LED lighting," *IEEE J. Sel. Areas Commun.*, vol. 27, no. 9, pp. 1654–1662, Dec. 2009.

[66] M. Ayman and L. Lampe, "Physical-layer security for MISO visible light communication channels," *IEEE J. Sel. Areas Commun.*, vol. 33, no. 9, pp. 1806–1818, Sep. 2015.

Ruowen Bai (Graduate Student Member, IEEE) received the B.S. degree from Nankai University in 2015, the M.E. degree (Hons.) from Tsinghua University, China, in 2018, and the Ph.D. degree in electrical and computer engineering from McMaster University, Canada, in 2021, where he is currently a Postdoctoral Fellow with the Department of Electrical and Computer Engineering. His current research interests include engineering optimization, modulation and signal processing for wireless communications and visible light communications, and digital communication algorithms.

Steve Hranilovic (Fellow, IEEE) received the B.A.Sc. degree (Hons.) in electrical engineering from the University of Waterloo, Canada, in 1997, and the M.A.Sc. and Ph.D. degrees in electrical engineering from the University of Toronto, Canada, in 1999 and 2003, respectively.

He is a Professor with the Department of Electrical and Computer Engineering, McMaster University, Hamilton, ON, Canada, and currently serves as the Associate Dean (Academic). From 2010 to 2011, he spent his research leave as a Senior Member and a Technical Staff with the Advanced Technology for Research in Motion, Waterloo, Canada. He has authored the book *Wireless Optical Communication Systems* (New York: Springer, 2004). His research interests are in the areas of free-space and optical wireless communications, digital communication algorithms, and electronic and photonic implementation of coding and communication algorithms.

Dr. Hranilovic was conferred as a University Scholar by McMaster University in 2016. He has served as an Associate Editor for the JOURNAL OF OPTICAL COMMUNICATIONS AND NETWORKING and an Editor for the IEEE TRANSACTIONS ON COMMUNICATIONS in the area of Optical Wireless Communications. He is a Fellow of Optica and is a licensed Professional Engineer in the Province of Ontario.

Zhaocheng Wang (Fellow, IEEE) received the B.S., M.S., and Ph.D. degrees from Tsinghua University in 1991, 1993, and 1996, respectively. From 1996 to 1997, he was a Postdoctoral Fellow with Nanyang Technological University, Singapore. From 1997 to 1999, he was a Research Engineer/Senior Engineer with OKI Techno Centre (Singapore) Pte. Ltd., Singapore. From 1999 to 2009, he was a Senior Engineer/Principal Engineer with Sony Deutschland GmbH, Germany. Since 2009, he has been a Professor with the Department of Electronic Engineering, Tsinghua University. He has authored or coauthored two books, which have been selected by IEEE Series on Digital and Mobile Communication and published by Wiley–IEEE Press. He has authored/coauthored more than 180 peer-reviewed journal articles. He holds 46 U.S./EU granted patents (23 of them as the first inventor). His research interests include wireless communications, millimeter wave communications, and optical wireless communications. He was a recipient of the ICC2013 Best Paper Award, the OECC2015 Best Student Paper Award, the 2016 IEEE Scott Helt Memorial Award, the 2016 IET Premium Award, the 2016 National Award for Science and Technology Progress (First Prize), the ICC2017 Best Paper Award, the 2018 IEEE ComSoc Asia–Pacific Outstanding Paper Award, and the 2020 IEEE ComSoc Leonard G. Abraham Prize. He is also an Associate Editor of the IEEE TRANSACTIONS ON COMMUNICATIONS, the IEEE SYSTEMS JOURNAL, and the IEEE OPEN JOURNAL OF VEHICULAR TECHNOLOGY. He was an Associate Editor of the IEEE TRANSACTIONS ON WIRELESS COMMUNICATIONS from 2011 to 2015, and the IEEE COMMUNICATIONS LETTERS from 2013 to 2016. He is a Fellow of the Institution of Engineering and Technology.